Chapter

Tribology of Ti-6Al-4V Alloy Manufactured by Additive Manufacturing

Auezhan Amanov

Abstract

In this study, the influence of ultrasonic nanocrystal surface modification (UNSM), which was applied as a post-additive manufacturing (AM), in terms of surface, tensile and tribological properties of Ti-6Al-4V alloy by selective laser melting (SLM) was investigated. Ti-6Al-4V alloy was subjected to UNSM at room and high temperatures (RT and HT). It was found that the UNSM enhanced the strength and reduced the roughness of the as-SLM sample, where both increased with increasing UNSM temperature. The UNSM bore influence on tribological properties, where the friction coefficient of the as-SLM sample reduced by about 25.8% and 305% and the wear resistance enhanced by about 41% and 246% at RT and HT, respectively. These are essentially attributed to the enhanced strength, smoothed surface and expelled pores from the surface. Based on SEM images, the damage caused by abrasive wear was the most observed in the wear track of the as-SLM sample than was caused by the highest wear rate. The UNSM temperature-dependent wear mechanisms were comprehensively investigated and elaborated based on the obtained experimental data and observed microstructural images. Indeed, a further investigation is required to improve the characteristics of as-SLM Ti-6Al-4V alloy to the wrought level due to the replacement possibility.

Keywords: roughness, strength, tribology, additive manufacturing, ultrasonic nanocrystal surface modification

1. Introduction

Ti-6Al-4V alloy is a metallic material that attracts much attention from many researchers due to its biocompatibility, good corrosion resistance and high specific strength. Due to these excellent properties, various components are made of Ti-6Al-4V alloy for biomedical and aerospace applications such as medical implants, aerospace crafts, gas turbines etc. [1, 2]. Recently, the advancement of additive manufacturing (AM) has been revelation for manufacturing customized parts with complex geometry in small volume, which is suitable for biomedical and aerospace industries. Selective laser melting (SLM) is one of AM that capable of processing a wide range of metals, alloys and metal matrix composites [3]. Therefore, this method is commonly used for fabrication of Ti-6Al-4V alloy components of those industries.

Attempts for improving their properties have been a critical subject for researchers for overall properties of SLM fabricated Ti-6Al-4V alloy parts [4]. It has been

reported that SLM fabricated components of nickel-based superalloys and titanium-based alloys are known to have several issues, such as cracking due to thermal stress by rapid heating and quenching [5, 6], poor surface finish and voids inside the material [6, 7], tensile residual stress, which causes deformation, cracks, and worsening of fatigue strength [4, 8], and columnar grain structures, which cause anisotropy in mechanical properties [9, 10]. To cope with these issues, various post-processing techniques have been applied such as surface milling for removing rough surface layers and possible cracks [8, 11], heat treatment for increasing toughness by phase transformation [12–15], laser polishing for decreasing surface roughness [16, 17], etc. Laser polishing reduced the roughness of laser AM TC4 and TC11 by about 75% and at the same time enhanced the surface micro-hardness of TC4 and TC11 by about 32% and 42%, respectively [18]. The other post-processing method that usually performed is hot isostatic pressing (HIP), which is capable of reducing the porosity and tensile residual stress of SLM fabricated Ti-6Al-4V alloy [19]. Post-heat treatments and HIP can solve some of those issues of SLM fabricated Ti-6Al-4V alloy, but the strength is significantly reduced. While laser polishing can increase the micro-hardness, but cannot solve the porosity-related issues and improve ductility.

For solving the aforementioned issues of metal AM, the application of surface treatment or modification technologies has been proposed, e.g., shot peening (SP), laser shock peening (LSP), and ultrasonic nanocrystal surface modification (UNSM). The application of SP showed a remarkable improvement in fatigue behavior of AlSi10Mg alloys fabricated by AM in the high cycle fatigue region [20]. A previous study reported that LSP can induce a deep level of compressive residual stress, which significantly improves the fatigue life of 316 L stainless steel fabricated by AM [21]. It was also reported that LSP provided more fatigue life improvement than SP, which is largely attributed to the depth of compressive residual stress.

UNSM is one of the mechanical surface modifications that utilizes an ultrasonic vibration energy to improve mechanical properties, tribological behavior, corrosion resistance and fatigue strength of various materials including AM fabricated materials. It was found earlier reported that the fatigue strength of SUS 304 shaft was improved by approximately 80% and the surface hardness is enhanced by both the grain refinement and the martensitic transformation after treatment by UNSM [22]. Furthermore, UNSM induced enhancement of surface hardness, compressive residual stress and grain refinement that resulted in improvement of fretting wear and frictional properties of commercially pure Ti and Ti-6Al-4V alloy [23]. The application of UNSM to AM fabricated materials has also been investigated. For example, Zhang et al. reported that electrically-assisted UNSM reduced the porosity and surface roughness, and enhanced the surface hardness of 3D printed Ti-6Al-4V alloy [24]. In our previous study on SLM fabricated 316 L stainless steel, it was reported that UNSM improved the mechanical properties, tribological behavior and corrosion resistance [25]. In general, UNSM reduces the surface roughness, increases the surface hardness, refines grain size and induces high compressive residual stress with the depth of hardened layer in the range of ~0.1 to ~0.3 mm [23, 25]. UNSM temperature-dependent surface hardness and phase transformation of wrought Ti-6Al-4V alloy were reported earlier [26], but the influence of UNSM temperature-dependent mechanical and tribological properties of AM fabricated Ti-6Al-4V alloy was not investigated yet. Therefore, in this study, the synergy effect of UNSM and local heat treatment (LHT) on the improvement of tensile and tribological properties of SLM fabricated Ti-6Al-4V alloy is investigated. The improvement in tensile and tribological properties after UNSM at different temperatures was compared with the results of the as-printed Ti-6Al-4V alloy.

2. Experimental procedure

2.1 Sample preparation

In this study, the sample made of Ti-6Al-4V alloy were fabricated by SLM (EOS M290, Germany) under the parameters listed in **Table 1**. **Figure 1** shows that the powder was spherical with a diameter of about 30–40 μm. Detailed information of SLM can be found in our previous study [25]. The hardness and yield strength of the as-printed samples were about 380 HV and 820 MPa, respectively. As for chemical composition, the content of Al and V was about 5.8 and 4.2 in wt.%, while the rest was Ti, respectively. The sample fabricated by SLM was used in as-printed state, which is hereinafter referred to as as-SLM, while the UNSM-treated samples at 25°C and 800°C are hereinafter referred to as UNSM-25 Degree-C and UNSM-800 Degree-C, respectively.

2.2 Application of UNSM technology

A UNSM is a cold-forging process that uses a tungsten carbide (WC) tip with a diameter of 2.38 mm to strike the sample surface at 20 kHz, which results in elasto-plastic and surface severe plastic deformation (S^2PD), and heating, whereas forming a nanostructured layer at RT and HT. Due to a small radius of the tip, the contact area with a sample is relatively small causing high contact pressure up to 30 GPa. Advantages of UNSM over other surface peening technologies for particular AM materials are that it smooths out the surface, which is usually rough after AM and also increases the strength simultaneously. Moreover, it somehow shrinkages pores due to the compressive strike. The samples were treated by UNSM using the following variables listed in **Table 2** at 25 and 800°C. The combination of UNSM and LHT was described in our previous study [27]. The main variables are important, while force being the most important because it's magnitude determines the intensity of strain hardening. The force is directly proportional to the surface hardness, the grain size, strain-hardened layer and the compressive residual stress. The roughness is inversely proportional to the force, while it is directly proportional to the feed-rate.

Laser power, W	Scan speed, mm/s	Hatching spacing, mm	Nominal layer thickness, μm
300	900	0.12	50

Table 1.
SLM parameters.

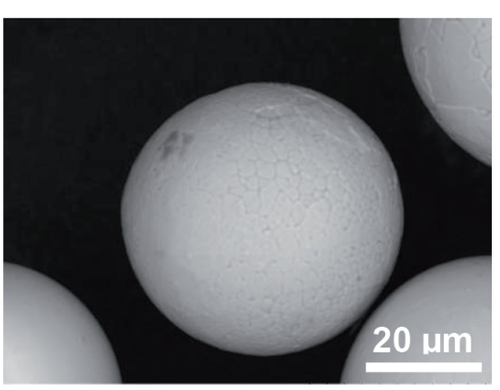

Figure 1.
SEM image of a single powder showing its shape and diameter.

Frequency, kHz	Amplitude, μm	Speed, mm/min	Force, N	Feed-rate, μm	Ball diameter, mm	Ball material	Temperature, °C
20	30	2000	40	10	2.38	WC	25, 800

Table 2.
UNSM treatment parameters.

Roughness data were obtained measured by non-contact laser scanning microscope (LSM: VK-X100 Series, Keyence, Japan). Hardness data were collected by hardness tester (MVK-E3, Mitutoyo, Japan) at a load of 300 gf. X-ray diffraction (XRD) was performed with a Cu Kα radiation (k = 1.54056 Å), a tube current of 40 mA and a voltage of 30 kV over the range of 30–90 with a scanning rate of 100/min by Bruker D8 Advance X-ray diffractometer. Compressive residual stress induced after UNSM was measured by portable device (μ-360 s, Pulstec, Japan), which is a nondestructive method. Tensile-induced fracture and wear mechanisms were investigated by SEM (JEOL, JSM-6010LA, Japan) and chemistry reacted at the contact interface was characterized by energy-dispersive X-ray spectroscopy (EDX: JEOL, JED2300, Japan).

3. Results and discussion

3.1 Surface topography

Figure 2 shows the top surface LSM images of the samples. In general, SLM fabricated samples demonstrated very rough surface due to the partially unmelted powders and also the presence of gas-induced pores on surface as shown in **Figure 2(a)**. The size of unmelted powders was found to be in the range of 30–40 μm, while the size of gas-induced pores was approximately 12 μm. The surface of the UNSM-25C sample is shown in **Figure 2(b)**. Obviously, the UNSM was able to impinge against those unmelted powders and to expel the pores from the surface, which was flattened at the end with no unmelted powders, pores and even cracks. In order to investigate the amalgamation of UNSM with thermal energy, the sample was treated by UNSM at 800°C. **Figure 2(c)** shows the surface of the UNSM-800C sample. The UNSM leaves the trace in the roughness of the surface that distorts by elasto-plastic deformation and S^2PD resulting in refining grains and creating cracks along the pathway of the WC tip. Doubtless, the unmelted powders and pores were not observed following the UNSM at 800°C, which led to the formation of some UNSM-induced isolated cracks noticed in **Figure 2(c)**. The initiated cracks are the indication of over-peening leading to an excessive strain hardening, where the amalgamated impact of UNSM and thermal energy resulted in surface degradation, and consequently imposing practical limitation in terms of surface quality rather than strength. An appearance of UNSM-induced isolated cracks can be explained in three stages: (1) the stage of strain hardening that consists of an intensive increase in surface roughness; (2) the stage of saturation, where a plastic shearing takes place leading to a reduction in dislocation density and cracks initiated; (3) the stage of surface damage, the integrity of surface is destroyed leading to an appearance of cracks, where the surface roughness increases. Actually, over-peening of surface peening technologies may deteriorate the surface integrity leading to a decrease in fatigue cycles or strength [28]. Over-peeing may cause inversion of stress that can reduce the compressive residual stress induced by UNSM. In this regard, it is always required to optimize the impact of surface peening technologies

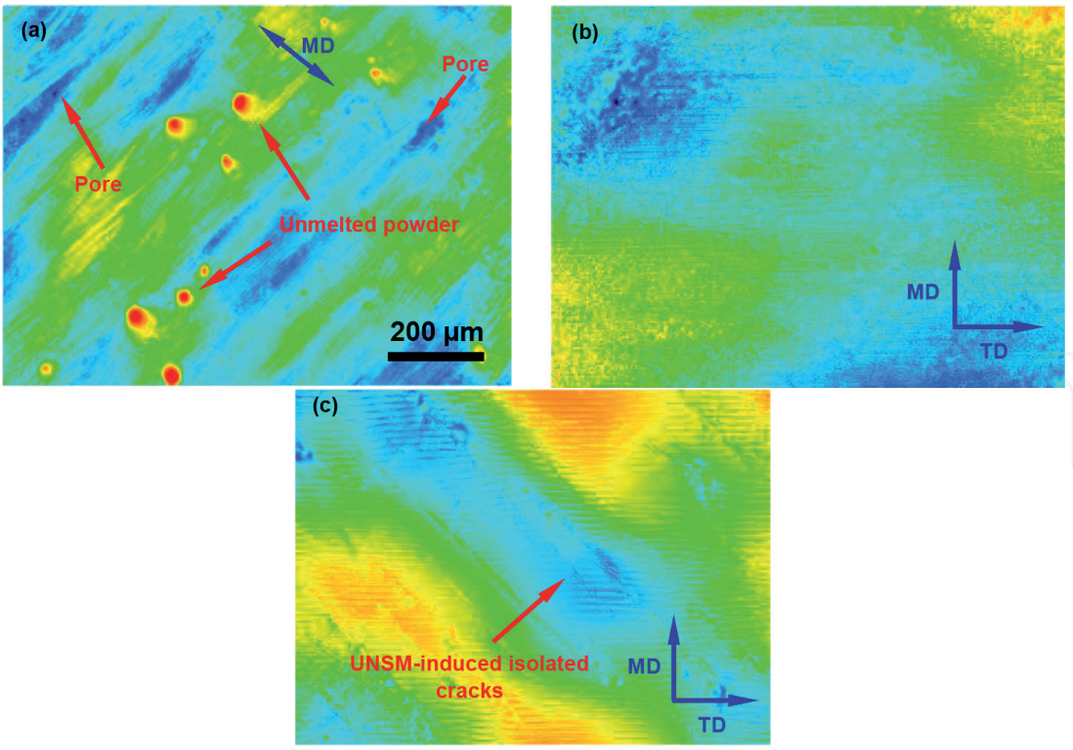

Figure 2.
Top surface LSM images of the as-SLM (a), UNSM-25C (b) and UNSM-800C (c) samples.

in order to avoid such crack initiation with the intention of preventing catastrophic failures of structures. There is still much improvements and optimizations in terms of microstructure- and ductility-based issued of AM materials to be done to be fully replaced with wrought alloys, but a progress in materials science and AM leading to overcome the faced challenge a couple of decades ago. Importantly, there is a way to get rid of from AM-based defects such as pore, unmelted and incompletely melted powders by HIP, which is highly-priced and time consuming that receiving a cautious welcome from various industries.

3.2 Surface integrity

Surface roughness measurement direction (MD) and UNSM treatment direction (TD) for each samples are shown in **Figure 2**. The surface roughness was measured in perpendicular direction to the UNSM TD. As mentioned in the previous subsection, a rough surface of AM fabricated samples is still considered as one of the main issues. One can be seen that the actual surface contained irregularities in the form of peaks and valleys. **Figure 3(a)** shows the comparison in surface roughness (R_a) profiles of the samples. The as-SLM sample had a roughness of about 9.541 μm, while it was drastically reduced up to 0.892 μm after UNSM at 25°C as shown in **Figure 3(a)**. The roughness of the UNSM-800C sample was 1.237 μm, which is about 7–8 times smoother than that of the as-SLM sample, but it is still rougher than UNSM-25C sample. A bit rougher surface of the UNSM-800C sample than that of the UNSM-25C sample is associated with plastic deformation during the heating that distorted the geometrically pattern resulting in increased the height of irregularities. In general, during the UNSM, a plastic deformation of the top and subsurface layers took place. Expelled pores and disposed peaks and valleys led to the reduction in surface roughness [25]. As those peaks and valleys between irregularities are notches that weaken the surface cause stress concentrations. Feed-rate pathways induced by UNSM and the presence of peaks and valleys are responsible

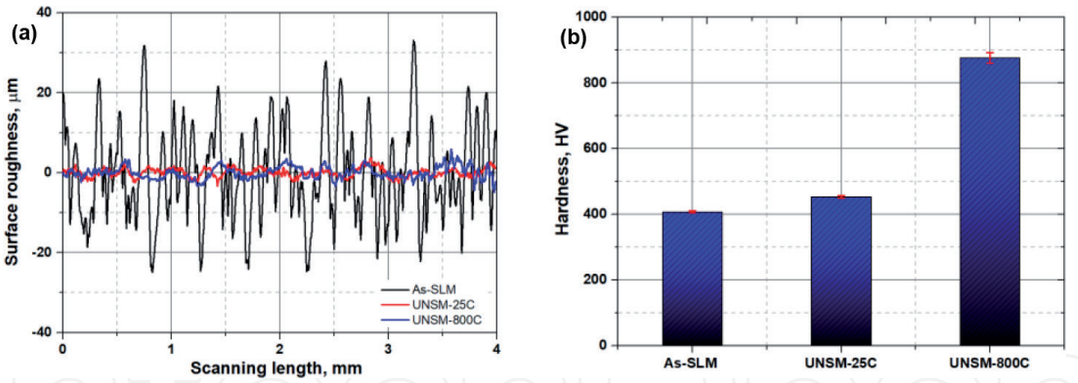

Figure 3.
Surface roughness (a) and hardness (b) of the as-SLM, UNSM-25C and UNSM-800C samples.

for the relatively rough surface of the UNSM-800C sample compared to that of the UNSM-25C sample. The level of plastic deformation increased and lessened flow eliminating with increasing temperature. Smoothed surface by UNSM at 25°C is beneficial to improving main structural properties such as tribology, corrosion and fatigue. Commonly, a surface quality of AM fabricated materials is very rough upon completion of AM [29]. This means that surface is required to be machined or finished. In this study, it is worth mentioning that the surface with no any additional machining or milling was treated by UNSM.

3.3 Surface hardening

Figure 3(b) shows the surface hardness measurement results of the samples. The average surface hardness of the as-SLM sample was approximately 396.4 HV, which increased up to 455.7 and 877.6 HV for the UNSM-25C and UNSM-800C samples, corresponding to a 13.1% and 221.3%, respectively. It is well documented in the literature that the increase in hardness is due to the combination of grain refinement by Hall-Petch expression and increased dislocation density, which are the results of elasto-plastic deformation and S^2PD took place in the top and subsurface layers [30]. The deformation usually refined the grains, which hinder further deformation and gradually diminishes with the depth of the surface layer. Moreover, Zhang et al. reported that the UNSM-induced work-hardening by plastic strain may also play a major role in increasing the hardness [31]. Moreover, in particular for AM materials, the expelled pores after peening technologies may be contributed to the increase in hardness [32].

3.4 Phase transformation

Figure 4 shows XRD patterns of the as-SLM, UNSM-25C and UNSM-800C samples. The change in diffraction peaks and phase transformation were confirmed by the relative intensity and the formation of a new peak after UNSM at 800°C. It was found that the intensity of all alpha phase peaks reduced except for (002) phase after UNSM at both 25 and 800°C. The intensity of alpha (101) phase increased for UNSM-800C sample and reduced for UNSM-25C sample. For as-SLM and UNSM-25C samples, the microstructure exhibited a full α/α`-phase, where α phase resulted from decomposition of α` during the SLM. For UNSM-800C sample, a precipitation of beta (110) phase was detected leading to a microstructure consisting of α and β phases as the temperature was higher than that of Ms. (575°C) [33]. Further, a broadening in full width at half maximum (FWHM) of the α peaks took place after UNSM, which led to the increase in dislocation density [27]. It is also obvious that

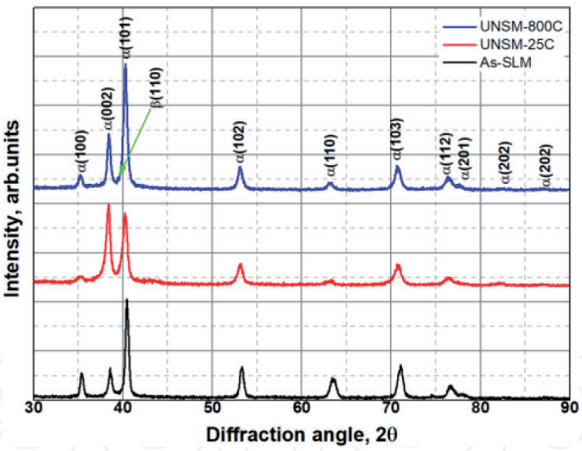

Figure 4.
XRD patterns of the as-SLM, UNSM-25C and UNSM-800C samples.

the UNSM increased the relative intensity of α (101) phase of the UNSM-800C sample as shown in **Figure 4**. Hence, it can be concluded that the UNSM resulted in grain size refinement. As a result, the FWHM values of the α (100) peak for the samples were listed in **Table 3**. It can be seen that FWHM of the as-SLM sample was broadened after UNSM at 25 °C. Furthermore, the FWHM of the UNSM-800C sample was found to be wider than that of the UNSM-25C sample, which signified that the refined grain after UNSM at 25°C was further refined after UNSM at 800°C. In general, it is well documented that the reduction in relative intensity of the peaks is responsible for the grain size refinement, which means that the UNSM refined the coarse grains into nano-grains, and also strain induced lattice distortion [34].

3.5 Tribology

Figure 5 shows the friction coefficient as a function of sliding cycles of the samples. It can be seen that all the samples came into contact with bearing steel (SAE 52100) underwent a running-in and steady-state frictional behavior. As shown in **Figure 5**, the friction coefficient of the as-SLM sample was found to be approximately 0.36 at the beginning of the friction test and increased continuously up to 0.52 for about 2000 cycles, which is considered as a running-in period. Then the friction coefficient continued being stable with a friction coefficient of 0.58 till the end of the test. **Figure 5** also shows the friction coefficient of the UNSM-25C sample. It was found that the friction coefficient demonstrated a similar friction behavior to the as-SLM sample, but the UNSM was able to reduce the friction coefficient in both the running-in and steady-state periods, where the friction coefficient was approximately 0.38 and 0.43, respectively. Overall, the friction behavior of the as-SLM sample was very highly fluctuated, which is associated with the initial rough surface. The frictional behavior of the UNSM-25C sample was relatively lower fluctuated, where the reduced surface roughness after UNSM is responsible for it. In addition,

Samples	FWHM	SD
As-SLM	0.46347	0.00738
UNSM-25C	0.59442	0.00628
UNSM-800C	0.77026	0.01093

Table 3.
Calculated FWHM results based on XRD pattern.

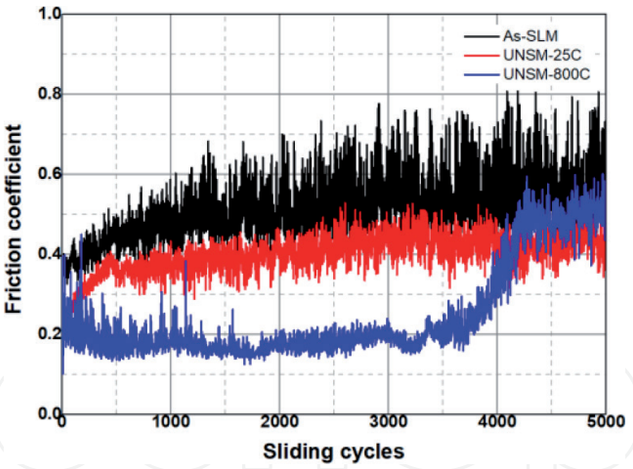

Figure 5.
Friction coefficient of the as-SLM, UNSM-25C and UNSM-800C samples.

as shown in **Figure 5**, the friction coefficient of the UNSM-800C sample was found to be approximately 0.19 at the beginning of the friction test and then continued to be stable for about 3600 cycles, which is considered as a running-in period. Then the friction coefficient gradually increased up to 0.51 and subsequently approached a stable friction coefficient till the end of the test. From the tribological tests, it was obvious that the as-SLM and UNSM-25C samples demonstrated a similar friction behavior, but the UNSM-800C sample extended the running-in period. Essentially, a lower friction coefficient was dominated by initial roughness of the samples, while an increase in hardness of the UNSM-800C sample, which came into first contact with the surface of counterface ball, had harder asperities that could increase the level of plastic deformation. A similar friction behavior was confirmed in the previous study on stainless steel 316 L that the friction coefficient was lower at the beginning of the test due to the initial surface roughness, where the asperities came into contact first and it deformed plastically with continuing reciprocating sliding [25]. Obtained friction coefficient results under dry conditions are in good consistency with the ultra-fined Ti-6Al-4V alloy fabricated by SLM [35].

The wear track dimensions of the samples were measured by 3D LSM as shown in **Figure 6**, which allowed to calculate the wear resistance based on the wear track width and depth dimensions. It can be seen that a significant difference was observed, where the wear track dimensions of the UNSM-800C sample was found to be the shallowest wear track compared to those of the as-SLM and UNSM-25C samples. The maximum peak-to-valley roughness height (R_{max}) of the wear track was about 226.3, 131.6 and 87.8 μm for the as-SLM, UNSM-25C and UNSM-800C samples, while no remarkable distinct in wear track width was observed due to the same contact pressure, respectively. As shown in the inset of **Figure 6**, the wear rate of the as-SLM sample was reduced from 3.57×10^{-8} to 1.48×10^{-8} and 8.70×10^{-9} $mm^3/N \times m$, corresponding to a ~ 41% and ~ 246% enhancement in wear resistance compared to those of the UNSM-25C and UNSM-800C samples, respectively. UNSM eliminated the effect of stress concentration in the inside of wear track, where it's depth did not exceed the thickness of strain-hardened layer containing refined nano-grains and compressive residual stress. Hence, the application of UNSM to the as-SLM sample at 25°C enhanced the wear resistance substantially due to the increase in hardness. Furthermore, a temperature increase of UNSM supplementary enhanced wear resistance. The reduction in surface roughness after UNSM led to the lower friction coefficient, while the increase in surface hardness was responsible for the higher wear resistance compared to that of the as-SLM sample. In addition, an induced compressive residual stress by UNSM

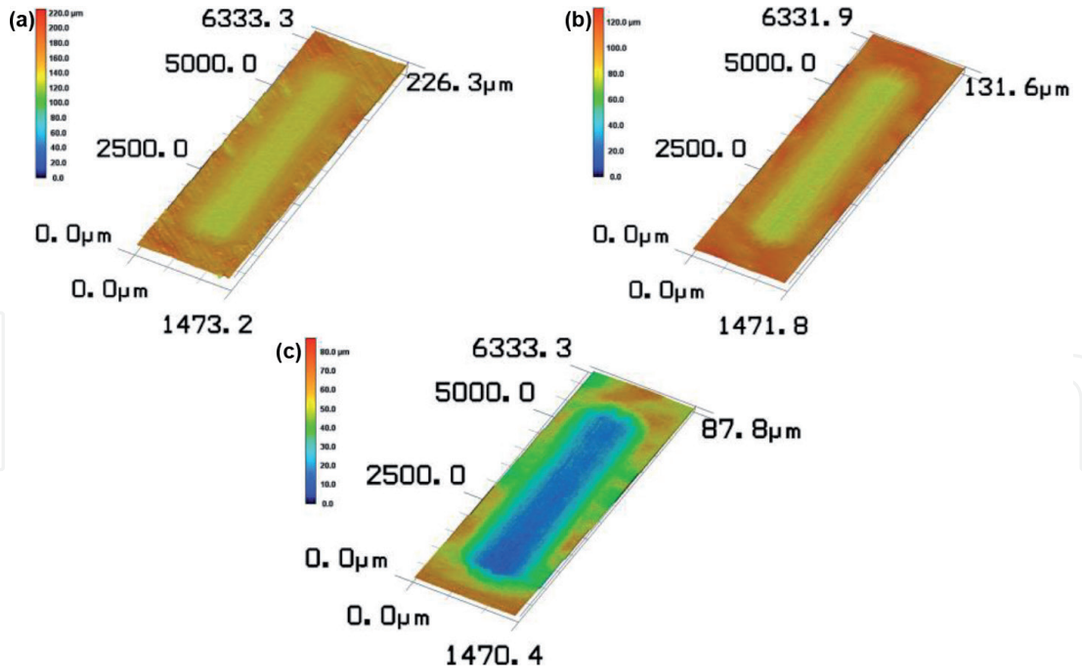

Figure 6.
3D LSM images of the as-SLM (a), UNSM-25C (b) and UNSM-800C (c) samples.

hindered the wear process [36]. As tribology considered as a system of two interacting surfaces, a wear scar of the counterface ball that came into contact with the as-SLM, UNSM-25C and UNSM-800C samples is shown in **Figure 7**. No significant difference in wear scar was observed, but the wear scar of the counterface ball that came into contact with the UNSM-800C sample was relatively smaller than those of the as-SLM and UNSM-25C samples. Beyond the wear scar of the counterface ball that came into contact with the as-SLM and UNSM-25C samples, accumulated debris were attached, while no any debris was found for the UNSM-800C sample. Finally, UNSM ensures improved surface integrity parameters and endurance of

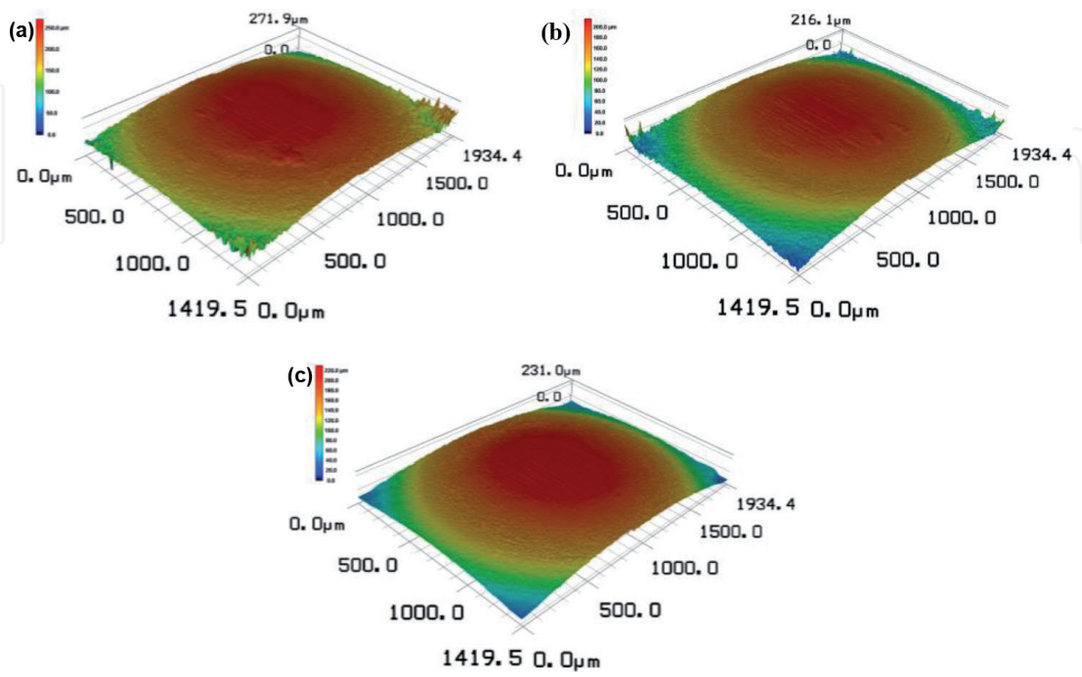

Figure 7.
3D LSM images of the counterface ball that came into contact with the as-SLM (a), UNSM-25C (b) and UNSM-800C (c) samples.

Ti-6Al-4V alloy fabricated by SLM with no subsequent process. Furthermore, it is of interest to note up that the fatigue strength of the UNSM-800C sample may be detrimental due to the presence of cracks on surface (see **Figure 2(c)**) induced by UNSM at HT of 800°C because of the presence of continuous stress leading to a crack propagation [37, 38].

Figure 8 shows the SEM images along with EDX results and oxidation distribution of the samples. It can be realized from SEM image in **Figure 8(a)** that the adhesive wear mechanism was found to be a dominant for the as-SLM sample as it is softer than that of the counterface ball, while a combination of abrasive and adhesive wear mechanisms was dominant for the UNSM-25C sample as shown in **Figure 8(b)**. An increase in temperature of UNSM resulted in changing wear mode as shown in **Figure 8(c)**, where the abrasive wear mechanisms took place for the UNSM-800C sample. Apart from those wear mechanisms, an oxidative wear mechanism came up in all the samples with different oxidation levels as shown in **Figure 8**. For instance, an oxide content over the wear track of the as-SLM sample was about 9.68%, while it was about 9.89% and 11.62% for the UNSM-25C and

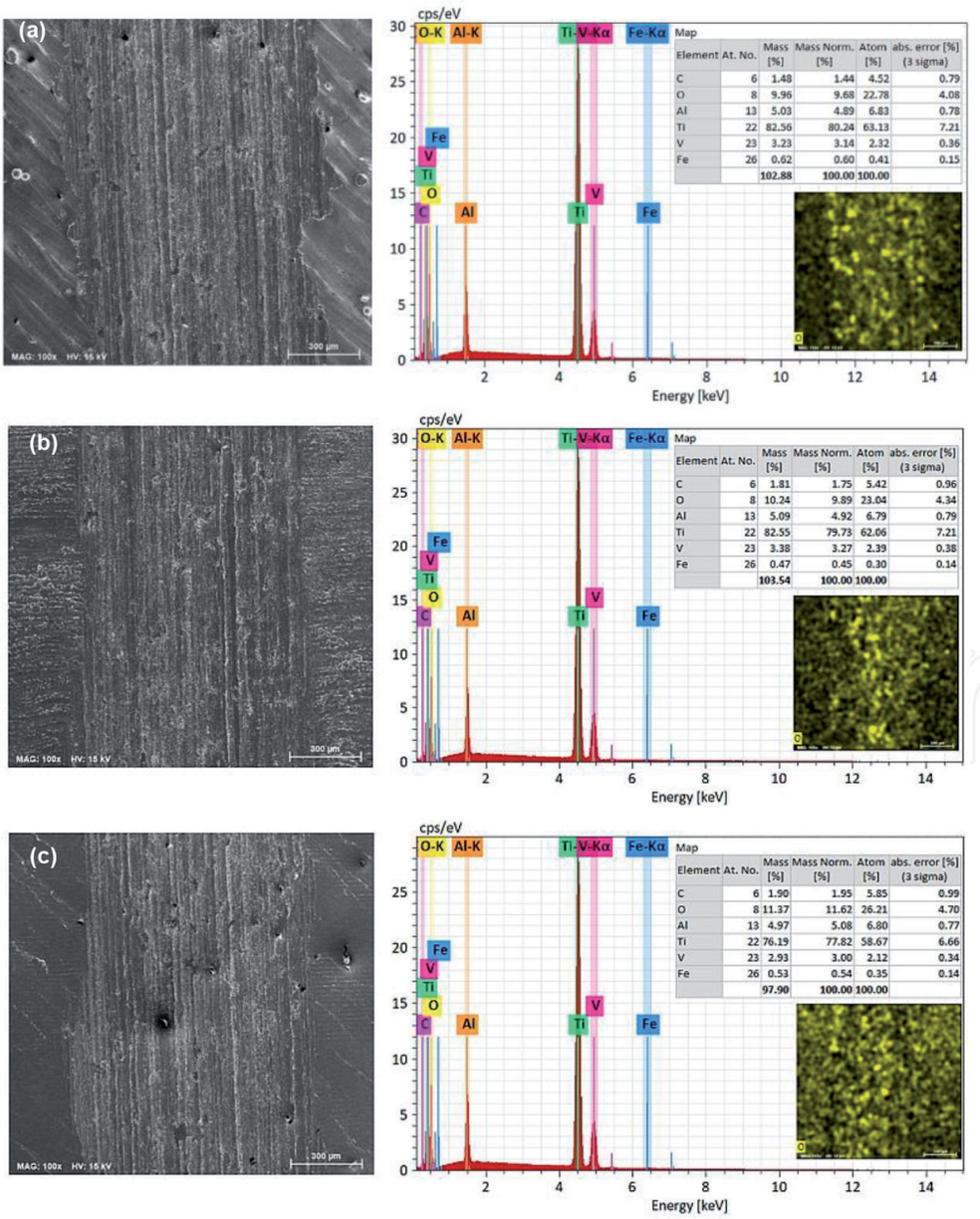

Figure 8.
SEM images along with EDX results of the as-SLM (a), UNSM-25C (b) and UNSM-800C (c) samples.

UNSM-800C samples, respectively. It is clear from oxide distribution mapping (see **Figure 8**) that the level of oxidation of the as-SLM and UNSM-25C samples was nearly consistent, but a relatively high level of oxidation occurred for the UNSM-800C sample. Zhang et al. reported that at a high temperature, a hardness of oxide layer become remarkably higher due to the presence of much oxide [39]. Hence, it is reasonable to hypothesize that it may significantly increase the wear resistance by obtaining low friction coefficient [40]. Typically, there is an advantage to forming an oxide layer between two mating surface as it prevents direct metal-to-metal contact resulting in lower friction coefficient and higher wear resistance. Furthermore, a nearly same amount of Fe, which was transferred from the counterface ball can be seen from the chemical composition table as shown in the inset of **Figure 8**. The presence of Fe along with occurred oxide may react together and form a ferrosoferric (Fe3O4) layer, which provides an advantageous environment for achieving a better tribological behavior and performance [27]. Furthermore, as the surface roughness of the samples deteriorated during the dry tribological tests as shown in **Figure 8**, where the post-test surface roughness of the UNSM-25C and UNSM800C samples was lower than that of the as-SLM sample. Hence, it can be considered that the surface roughness after dry tribological tests is much important than post-surface treatment because the surface during the dry tribological tests comprises a number of grooves of different depth and sharpness – causing local stress concentrations and decreasing the wear resistance.

4. Conclusions

In this study, the influence of UNSM on the surface, tensile and tribological properties of Ti-6Al-4V alloy fabricated by SLM was evaluated. The as-SLM sample had a roughness of about 9.541 μm, which was drastically reduced up to 0.892 and 3.058 μm after UNSM at 25 and 800°C. The average surface hardness of the as-SLM sample was approximately 396.4 HV, which increased up to 455.7 and 877.6 HV for the UNSM-25C and UNSM-800C samples, corresponding to a 13.1% and 221.3% increase, respectively. The surface residual stress of both the UNSM-25C and UNSM-800C samples was transferred into compressive residual stress. The as-SLM sample demonstrated lower YS and UTS than UNSM-25C and UNSM-800C samples, but its elongation was shorter than that of the UNSM-25C sample and longer than that of the UNSM-800C sample. YS and UTS of the UNSM-25C sample was lower and higher than that of the UNSM-800C sample, while the elongation was also longer than that of the UNSM-800C sample. Friction coefficient of the as-SLM sample was reduced by the application of UNSM at 25 °C by about 25.8%, and it further reduced by about 305% increasing the UNSM temperature up to 800 °C. The wear rate of the as-SLM sample was reduced by about 41% and 246% compared to those of the UNSM-25C and UNSM-800C samples, respectively. As a main conclusion, a UNSM at RT and HT may be applied to Ti-6Al-4V alloy fabricated by SLM with the intention of enhancing tensile and tribological properties of various components in aerospace and biomedical applications. Indeed, a further investigation is required to improve the properties and performance of Ti-6Al-4V alloy fabricated by SLM to the wrought level due to the replacement possibility.

Acknowledgements

This study was supported by the Industrial Technology Innovation Development Project of the Ministry of Commerce, Industry and Energy, Rep. Korea (No.

20010482). This research was supported by Basic Science Research Program through the National Research Foundation of Korea (NRF) funded by the Ministry of Education (No. 2020R1I1A3074119).

Conflict of interest

The author has no conflict of interest to declare.

Author details

Auezhan Amanov
Sun Moon University, Asan, South Korea

*Address all correspondence to: avaz2662@sunmoon.ac.kr

References

[1] Bagehorn S, Wehr J, Maier HJ. Application of mechanical surface finishing processes for roughness reduction and fatigue improvement of additively manufactured Ti-6Al-4V parts. Int. J. Fatigue. 2017;102:135-142. DOI: 10.1016/j.ijfatigue.2017.05.008

[2] Gorsse S, Hutchinson C, Gouné M, Banerjee R. Additive manufacturing of metals: A brief review of the characteristic microstructures and properties of steels, Ti-6Al-4V and high-entropy alloys. Sci. Technol. Adv. Mater. 2017;18:584-610. DOI: 10.1080/14686996.2017.1361305

[3] Gu D, Hagedorn YC, Meiners W, Meng G, Batista RJS, Wissenbach K, Poprawe R. Densification behavior, microstructure evolution, and wear performance of selective laser melting processed commercially pure titanium. Acta Materialia. 2012;60:3849-3860. DOI: 10.1016/j.actamat.2012.04.006

[4] Thijs L, Verhaeghe F, Craeghs T, Humbeeck JV, Kruth JP. A study of the microstructural evolution during selective laser melting of Ti–6Al–4V. Acta Materialia. 2010;58:3303-3312. DOI: 10.1016/j.actamat.2010.02.004.

[5] Abe F, Osakada K, Shiomi M, Uematsu K, Matsumoto M. The manufacturing of hard tools from metallic powders by selective laser melting. J. Mater. Process. Technol. 2001;111:210-213. DOI: 10.1016/S0924-0136(01)00522-2.

[6] Mumtaz KA, Erasenthiran P, Hopkinson N. High density selective laser melting of Waspaloy®. J. Mater. Process. Technol. 2008;195:77-87. DOI: 10.1016/j.jmatprotec.2007.04.117.

[7] Ma C, Andani MT, Qin H, Moghaddam NS, Ibrahim H, Jahadakbar A, Amerinatanzi A, Ren Z, Zhang H, Doll GL, Dong Y, Elahinia M, Ye C. Improving surface finish and wear resistance of additive manufactured nickel-titanium by ultrasonic nanocrystal surface modification. J. Mater. Process. Technol. 2017;249:433-440. DOI: 10.1016/j.jmatprotec.2017.06.038.

[8] Shiomi M, Osakada K, Nakamura K, Yamashita T, Abe F. Residual stress within metallic model made by selective laser melting process. CIRP Annals. 2004;53:195-198. DOI: 10.1016/S0007-8506(07)60677-5.

[9] Qiu C, Adkins NJE, Attallah MM. Microstructure and tensile properties of selectively laser-melted and of HIPed laser-melted Ti–6Al–4V. Mater. Sci. Eng. A. 2013;578:230-239. DOI: 10.1016/j.msea.2013.04.099.

[10] Vilaro T, Colin C, Bartout JD, Nazé L, Sennour M. Microstructural and mechanical approaches of the selective laser melting process applied to a nickel-base superalloy. Mater. Sci. Eng. A. 2012;534:446-451. DOI: 10.1016/j.msea.2011.11.092.

[11] Osakada K, Shiomi M. Flexible manufacturing of metallic products by selective laser melting of powder. International J. Mach. Tools Manuf. 2006;46:1188-1193. DOI: 10.1016/j.ijmachtools.2006.01.024.

[12] Lee KA, Kim YK, Yu JH, Park SH, Kim MC, Effect of heat treatment on microstructure and impact toughness of Ti-6Al-4V manufactured by selective laser melting process. Arch. of Metal. Mater. 2017;62:1341-1346. DOI: 10.1515/amm-2017-0205.

[13] Vilaro T, Colin C, Bartout JD. As-fabricated and heat-treated microstructures of the Ti-6Al-4V alloy processed by selective laser melting. Metal. Mater. Trans. A.

2011;42:3190-3199. DOI: 10.1007/s11661-011-0731-y.

[14] Ter Haar GM, Becker T, Blaine DC. Influence of heat treatments on the microstructure and tensile behaviour of selective laser melting-produced Ti-6Al-4V parts. S. Afr. J. Ind. Eng. 2016;27. DOI: 10.7166/27-3-1663.

[15] Vrancken B, Thijs L, Kruth JP, Van Humbeeck J. Heat treatment of Ti6Al4V produced by selective laser melting: Microstructure and mechanical properties. J. Alloys Comp. 2012;541:177-185. DOI: 10.1016/j.jallcom.2012.07.022.

[16] Bhaduri D, Penchev P, Batal A, Dimov S, Soo SL, Sten S, Harrysson U, Zhang Z, Dong H. Laser polishing of 3D printed mesoscale components. Appl. Surf. Sci. 2017;405:29-46. DOI: 10.1016/j.apsusc.2017.01.211.

[17] Rosa B, Mognol P, Hascoët J. Laser polishing of additive laser manufacturing surfaces. J. Laser Appl. 2015;27:S29102. DOI: 10.2351/1.4906385.

[18] Ma CP, Guan YC, Zhou W. Laser polishing of additive manufactured Ti alloys/ Opt. Lasers Eng. 2017;93:171-177. DOI: 10.1016/j.optlaseng.2017.02.005.

[19] Leuders S, Thöne M, Riemer A, Niendorf T, Tröster T, Richard HA, Maier HJ. On the mechanical behaviour of titanium alloy TiAl6V4 manufactured by selective laser melting: Fatigue resistance and crack growth performance. Int. J. Fatigue. 2013;48:300-307. DOI: 10.1016/j.ijfatigue.2012.11.011.

[20] Uzan NE, Ramati S, Shneck R, Frage N, Yeheskel O. On the effect of shot-peening on fatigue resistance of AlSi10Mg specimens fabricated by additive manufacturing using selective laser melting (AM-SLM). Addit. Manuf. 2018;21:458-464. DOI: 10.1016/j.addma.2018.03.030.

[21] Hackel L, Rankin JR, Rubenchik A, King WE, Matthews M. Laser peening: A tool for additive manufacturing post-processing. Addit. Manuf. 2018;24:67-75. DOI: 10.1016/j.addma.2018.09.013.

[22] Yasuoka M, Wang P, Zhang K, Qiu Z, Kusaka K, Pyoun YS, Murakami R. Improvement of the fatigue strength of SUS304 austenite stainless steel using ultrasonic nanocrystal surface modification. Surf. Coat. Technol. 2013;218:93-98. DOI: 10.1016/j.surfcoat.2012.12.033.

[23] Amanov A, Cho IS, Kim DE, Pyun YS. Fretting wear and friction reduction of CP titanium and Ti-6Al-4V alloy by ultrasonic nanocrystalline surface modification. Surf. Coat. Technol. 2012;207:135-142. DOI: 10.1016/j.surfcoat.2012.06.046.

[24] Zhang H, Zhao J, Liu J, Qin H, Ren Z, Doll GL, Dong Y, Ye C. The effects of electrically-assisted ultrasonic nanocrystal surface modification on 3D-printed Ti-6Al-4V alloy. Addit. Manuf. 2018;22:60-68. DOI: 10.1016/j.addma.2018.04.035.

[25] Amanov A. Effect of local treatment temperature of ultrasonic nanocrystalline surface modification on tribological behavior and corrosion resistance of stainless steel 316L produced by selective laser melting. Surf. Coat. Technol. 2020;398:126080. DOI: 10.1016/j.surfcoat.2020.126080.

[26] Amanov A, Urmanov B, Amanov T, Pyun YS. Strengthening of Ti-6Al-4V alloy by high temperature ultrasonic nanocrystal surface modification technique. Mater. Lett. 2017;196:198-201. DOI: 10.1016/j.matlet.2017.03.059.

[27] Amanov A, Pyun YS. Local heat treatment with and without ultrasonic nanocrystal surface modification of Ti-6Al-4V alloy: Mechanical and tribological properties. Surf. Coat.

Technol. 2017;326(A):343-354. DOI: 10.1016/j.surfcoat.2017.07.064.

[28] Bhuvaraghan B, Srinivasan SM, Maffeo B. Optimization of the fatigue strength of materials due to shot peening: A Survey. Int. J. Struct. Chang. Solids. 2010;2(2):33-63.

[29] Iquebal AS, Sagapuram D, Bukkapatnam STS. Surface plastic flow in polishing of rough surfaces. Sci. Rep. 2019;9:10617. DOI: 10.1038/s41598-019-46997-w.

[30] Zhang Q , Xie J, London T, Griffiths D, Bhamji I, Oancea V. Estimates of the mechanical properties of laser powder bed fusion Ti-6Al-4V parts using finite element models. Mater. Design. 2019;169:107678. DOI: 10.1016/j.matdes.2019.107678.

[31] Zhang H, Chiang R, Qin H, Ren Z, Hou X, Lin D, Doll GL, Vasudevan VK, Dong Y, Ye C. The effects of ultrasonic nanocrystal surface modification on the fatigue performance of 3D-printed Ti64. International Journal of Fatigue. 2017;103:136-146. DOI: 10.1016/j.ijfatigue.2017.05.019.

[32] Kahlin M, Ansell H, Basu D, Kerwin A, Newton L, Smith B, Moverare JJ. Improved fatigue strength of additively manufactured Ti6Al4V by surface post processing. Int. J. Fatigue. 2020;134:105497. DOI: 10.1016/j.ijfatigue.2020.105497.

[33] Yang Y, Liu YJ, Chen J, Wang HL, Zhang ZQ , Lu YJ, Wu SQ , Lin JX. Crystallographic features of α variants and β phase for Ti-6Al-4V alloy fabricated by selective laser melting. Mater. Sci. Eng. A. 2017;707:548-558. DOI: 10.1016/j.msea.2017.09.068.

[34] Ye C, Telang A, Gill AS, Suslov S, Idell Y, Zweiacker K, Wiezorek JMK, Zhou Z, Qian D, Mannava SR, Vasudevan VK. Gradient nanostructure and residual stresses induced by ultrasonic nanocrystal surface modification in 304 austenitic stainless steel for high strength and high ductility. Mater. Sci. Eng. A. 2014;613:274-288. DOI: 10.1016/j.msea.2014.06.114.

[35] Li Y, Song L, Xie P, Cheng M, Xiao H. Enhancing hardness and wear performance of laser additive manufactured Ti6Al4V alloy through achieving ultrafine microstructure. Materials. 2020;13:1210. doi:10.3390/ma13051210.

[36] Wang C, Jiang C, Chen M, Wang L, Liu H, Ji V. Residual stress and microstructure evolution of shot peened Ni-Al bronze at elevated temperatures. Mater. Sci. Eng. A. 2017;707:629-635. DOI: 10.1016/j.msea.2017.09.098.

[37] Fotovvati B , Namdari N, Dehghanghadikolaei A. Fatigue performance of selective laser melted Ti6Al4V components: State of the art. Mater. Res. Express. 2018;6(1): 012002. DOI: 10.1088/2053-1591/aae10e

[38] Edwards P, Ramulu M. Fatigue performance evaluation of selective laser melted Ti-6Al-4V. Mater. Sci. Eng. A. 2014;598:327-337. DOI: 10.1016/j.msea.2014.01.041.

[39] Zhang QY, Zhou Y, Wang L, Cui XH, Wang SQ. Investigation on tribo-layers and their function of a titanium alloy during dry sliding. Tribol. Int. 2016;94:541-549. DOI: 10.1016/j.triboint.2015.10.018.

[40] Balla VK, Soderlind J, Bose S, Bandyopadhyay A. Microstructure, mechanical and wear properties of laser surface melted Ti6Al4V alloy. J. Mech. Behav. Biomed. Mater. 2014;32:335-344. DOI: 10.1016/j.jmbbm.2013.12.001.